

**This is an electronic reprint of the original article.
This reprint *may differ* from the original in pagination and typographic detail.**

Author(s): Ikonen, Joni; Salmilehto, Juha; Möttönen, Mikko

Title: Energy-efficient quantum computing

Year: 2017

Version:

Please cite the original version:

Ikonen, J., Salmilehto, J., & Möttönen, M. (2017). Energy-efficient quantum computing. npj Quantum Information, 3, Article 17. <https://doi.org/10.1038/s41534-017-0015-5>

All material supplied via JYX is protected by copyright and other intellectual property rights, and duplication or sale of all or part of any of the repository collections is not permitted, except that material may be duplicated by you for your research use or educational purposes in electronic or print form. You must obtain permission for any other use. Electronic or print copies may not be offered, whether for sale or otherwise to anyone who is not an authorised user.

ARTICLE OPEN

Energy-efficient quantum computing

Joni Ikonen^{1,2}, Juha Salmilehto² and Mikko Möttönen^{1,3}

In the near future, one of the major challenges in the realization of large-scale quantum computers operating at low temperatures is the management of harmful heat loads owing to thermal conduction of cabling and dissipation at cryogenic components. This naturally raises the question that what are the fundamental limitations of energy consumption in scalable quantum computing. In this work, we derive the greatest lower bound for the gate error induced by a single application of a bosonic drive mode of given energy. Previously, such an error type has been considered to be inversely proportional to the total driving power, but we show that this limitation can be circumvented by introducing a qubit driving scheme which reuses and corrects drive pulses. Specifically, our method serves to reduce the average energy consumption per gate operation without increasing the average gate error. Thus our work shows that precise, scalable control of quantum systems can, in principle, be implemented without the introduction of excessive heat or decoherence.

npj Quantum Information (2017)3:17; doi:10.1038/s41534-017-0015-5

INTRODUCTION

Quantum bits, or qubits,¹ have been realized using, for example, superconducting circuits,^{2–4} quantum dots,^{5, 6} trapped ions,^{7, 8} single dopants in silicon,⁹ and nitrogen vacancy centers.¹⁰ The state of a qubit is affected by various sources of error such as finite qubit lifetime, measurement imperfections, non-ideal initialization, and imprecise external control. Provided that these errors are below a certain threshold, they can be corrected with quantum error correction codes,^{4, 11, 12} which encode the information of a logical qubit into an ensemble of physical qubits. Error correction codes with exceptionally high thresholds, such as surface codes,¹² typically require thousands of physical qubits for each fault-tolerant logical qubit, which calls for a vast amount of physical resources to realize a computationally useful quantum computer.

Consequently, extensions of the already demonstrated experimental techniques to a large-scale solid-state quantum computer introduces practical scaling challenges that are not pronounced in the present prototypes. Along with physical volume limitations, these issues include excessive heat conduction through the vast number of required transmission lines and harmful dissipation at attenuators. This motivates the investigation of control methods alternative to the present standards, such as generation or redistribution of the qubit control pulses at the chip level. See [Supplementary Information](#) for more detailed discussion.

Although the overhead related to quantum error correction can be decreased by implementing more accurate operations, it is known that the quantum-mechanical uncertainties in very weak control pulses significantly increase the gate errors.^{13–19} In the case of a resonant control pulse, this type of error is inversely proportional to the pulse energy, and hence may, in principle, pose a trade-off in the power management of the quantum computer. Thus it is interesting to study the fundamental limitations of the quantum gate fidelity arising from finite pulse energy.

In this work, we first derive the greatest lower bound for the single-pulse gate error within the resonant Jaynes–Cummings

model.^{20, 21} The inevitable error originates from the quantum nature of the drive pulse and becomes dominant in the regime of low drive powers. In contrast to previous work,^{15, 16, 19} our constructive derivation does not assume any particular state of the system and is applicable to qubit rotations of arbitrary angles. In addition to the lower bound itself, our method naturally finds the bosonic quantum states of the pulses that reach the bound. We explicitly show that single-qubit rotations are optimally realized by applying a certain amount of squeezing to coherent states.

We also find that back-action-induced correlations between the control pulse and the controlled qubit can be transferred to auxiliary qubits (see also Refs. 22–24). Thus, we propose a control protocol where multiple gates are generated with a single control pulse which is frequently refreshed using auxiliary qubits. Whereas previous studies suggest that it is not possible to save energy by reusing control pulses without sacrificing the minimum gate fidelity,¹⁶ our method exhibits orders of magnitude smaller energy consumption with no drop in the average gate fidelity.

RESULTS

Semiclassical model

Let us first review the semiclassical formalism of single-qubit control and the resulting gate errors. The state of a qubit can be represented as a Bloch vector constrained inside a unit sphere, see Fig. 1. Single-qubit logic gates R_θ , realized using, e.g., microwave pulses, rotate the Bloch vector by θ about the axis R . Assuming that the control pulse is a classical waveform in resonance with the qubit transition energy $\hbar\omega$, the system may be described in the rotating frame using a semiclassical interaction Hamiltonian of the form²⁵

$$\hat{H}_{\text{int}}^{\text{cl}}(t) = \hbar g(t)(a|e\rangle\langle g| + a^*|g\rangle\langle e|), \quad (1)$$

where $|g\rangle$ and $|e\rangle$ denote the ground and excited states of the qubit, respectively, $a = |a|e^{i\phi}$ represents the classical amplitude $|a|$ and phase ϕ of the control field, $g(t)$ is the coupling constant

¹QCD Labs, COMP Center of Excellence, Department of Applied Physics, Aalto University, P.O. Box 13500, Aalto FI-00076, Finland; ²Department of Physics, Yale University, New Haven, Connecticut 06520, USA and ³Department of Mathematical Information Technology, University of Jyväskylä, P.O. Box 35, Jyväskylä FI-40014, Finland
Correspondence: Joni Ikonen (joni.2.ikonen@aalto.fi)

Received: 20 September 2016 Revised: 3 February 2017 Accepted: 18 February 2017

Published online: 14 April 2017

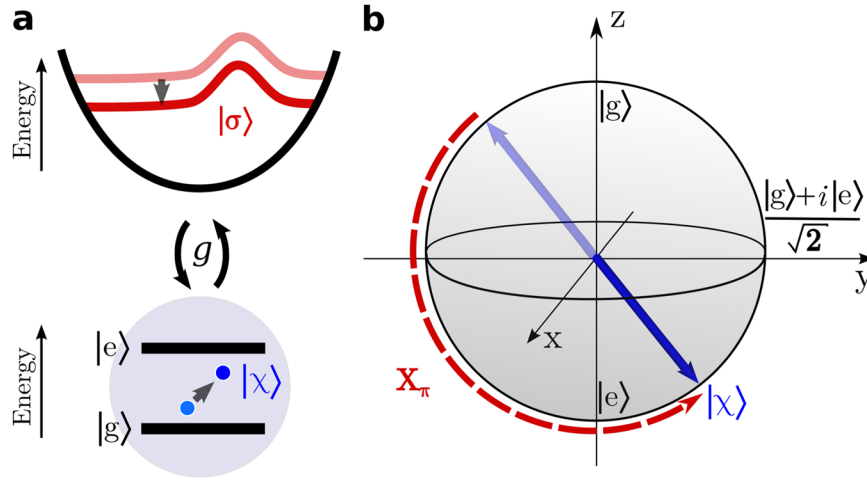


Fig. 1 Model system. **a** Ideal two-level system (bottom) interacting with a harmonic oscillator (top). **b** Bloch vector representation of the qubit state $|\chi\rangle$ and an example X_π rotation

including the pulse envelope, and \hbar is the reduced Planck constant. The gate R_θ is implemented by choosing the interaction time T and the pulse envelope such that they satisfy $2|a|\int_0^T g(t)dt = \theta$. For example, setting $\theta = \pi$ and R along the x -axis, the temporal evolution operator $\hat{U}_{cl} = \exp[-i\int_0^T \hat{H}_{int}^{cl}(t)dt/\hbar]$ becomes $\hat{U}_{cl} = -i\hat{\sigma}_x$, where $\hat{\sigma}_x = |e\rangle\langle g| + |g\rangle\langle e|$ is the Pauli X -operator. Thus, up to a redundant global phase factor, the interaction implements a perfect NOT gate X_π .

We assess gate errors by utilizing the state transformation error

$$\mathcal{E}_{cl}(\vartheta, \varphi) = 1 - |\langle \chi_0 | \hat{K}^\dagger \hat{U}_{cl} | \chi_0 \rangle|^2, \quad (2)$$

where the initial qubit state is given by $|\chi_0\rangle = \cos(\frac{\vartheta}{2})|g\rangle + \sin(\frac{\vartheta}{2})e^{i\varphi}|e\rangle$ and \hat{K} is the desired gate. In general, the qubit state is unknown during the computation, and therefore we choose not to restrict our analysis to any specific state. Instead, we study the average of a given error measure \mathcal{E}_i over a uniform state distribution on the Bloch sphere, generally given by

$$\bar{\mathcal{E}}_i = \frac{1}{4\pi} \int_0^\pi \int_0^{2\pi} \mathcal{E}_i(\vartheta, \varphi) \sin \vartheta d\vartheta d\varphi. \quad (3)$$

Semiclassically, a source of gate error arises from uncertainties in the phase and the photon number n , which are, for small-phase fluctuations, fundamentally bounded by quantum mechanics through the minimal uncertainty relation²⁶ $\Delta n \Delta \phi = 1/2$. Thus we consider a control pulse with an average of $\bar{n} = |a|^2$ photons and minimal uncertainties $\Delta n = \sqrt{\bar{n}}e^{-r}$ and $\Delta \phi = e^r/(2\sqrt{\bar{n}})$, where r is a free squeezing parameter. These uncertainties carry on to the temporal evolution operator \hat{U}_{cl} , and we find from Eq. (3) that the average gate error becomes inversely proportional to the photon number. For the X_π gate for example, we obtain the average gate error $\bar{\mathcal{E}}_{cl} = (4e^{2r} + \pi^2 e^{-2r})/(24\bar{n})$ in the limit $\bar{n} \rightarrow \infty$. Interestingly, the error is minimized with a finite squeezing parameter $r = \ln \sqrt{\pi/2}$, a result reproduced in the full quantum treatment below. An alternative qubit-independent error quantity is the maximum gate error given by $\mathcal{E}_{max} = \max_{\vartheta, \varphi} \mathcal{E}(\vartheta, \varphi)$, which obeys a similar $1/\bar{n}$ -dependence.^{19, 14}

Quantum bound for gate error

Let us proceed to the full quantum treatment, where the gate operation arises from the quantum-mechanical interaction between the qubit and a single bosonic mode referred to as the drive. Utilization of such quantum drive²⁷ allows us to account for the changes in its state arising from the interaction with the qubit.

In practice, qubits are also driven by propagating photons described by a continuum of modes, but such arrangements do not save energy in comparison to a well-controlled single mode (see [Supplementary Information](#)). Hence our description below is expected to yield a fundamental lower bound for the energy needed for controlling a single qubit at a given fidelity.

To account for the quantum properties of the drive, we replace the classical Hamiltonian of Eq. (1) with the resonant Jaynes–Cummings Hamiltonian²⁵ and define the transformation error as (see Methods)

$$\mathcal{E}[\hat{\chi}_0, \hat{\chi}(T)] = 1 - \text{Tr}[\hat{\chi}(T)\hat{K}\hat{\chi}_0\hat{K}^\dagger], \quad (4)$$

where $\hat{\chi}_0$ and $\hat{\chi}(T)$ are the density operators of the qubit before and after the interaction with the drive pulse, respectively.

We are able to solve the drive states that minimize the average or maximum gate error for a given interaction time and a desired rotation R_θ about an axis in the xy -plane. We find that the error-minimizing drive states are solutions of eigenvalue equations of the form

$$\hat{F}_i |\sigma_0^{\text{opt}, i}\rangle = f_i |\sigma_0^{\text{opt}, i}\rangle, \quad (5)$$

where \hat{F}_i is an operator constructed from the temporal evolution operator, the target gate, and the initial qubit state (see Methods and [Supplementary Information](#) for detailed derivations). The operator \hat{F}_i , and hence the optimal drive state, take different forms depending on whether we choose to minimize the average gate error ($i = \text{avg}$) or the maximum gate error ($i = \text{max}$). By definition, the optimal states $|\sigma_0^{\text{opt}, i}\rangle$ provide the greatest lower bound for the error \mathcal{E}_i .

We solve this eigenvalue equation numerically. Examples of fidelity-optimal solutions are shown in Fig. 2a using the Wigner pseudo-probability function.²⁸ We note that the numerically obtained states are essentially identical to the squeezed coherent states $|\alpha, r\rangle = \hat{D}(\alpha)\hat{S}(r)|0\rangle$, where $\hat{D}(\alpha) = e^{a\hat{a}^\dagger - \alpha^* \hat{a}}$ and $\hat{S}(r) = e^{\frac{1}{2}r(\hat{a}^2 - \frac{1}{2}(\hat{a}^\dagger)^2)}$ are the displacement and squeezing operators, respectively.²⁸ The difference between the numerical and the exact squeezed state decreases rapidly with increasing α , and the difference in the gate error produced by these states is negligible. Importantly, the numerical solutions possess the correct amplitude and phase to satisfy the timing condition $2gT|a| = \theta$ and to set the desired direction of the rotation axis, without imposing them explicitly. Furthermore, the average errors, as well as the

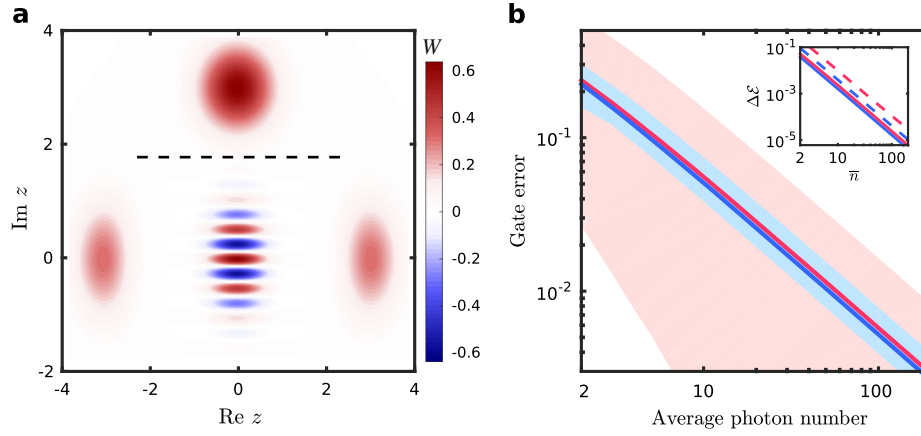


Fig. 2 Optimal drive states and the resulting error. **a** Numerically solved initial drive states $|\sigma_0^{\text{opt,avg}}\rangle$ that minimize the average error of rotations $Y_{\pi/2}$ and X_{π} as Wigner distributions above and below the dashed line, respectively. The Wigner function is defined as $W(z) = \frac{2}{\pi} \text{Tr}_D[\hat{D}(-z)|\sigma_0^{\text{opt}}\rangle\langle\sigma_0^{\text{opt}}|\hat{D}(z)e^{i\pi a^\dagger a}]$, where $\hat{D}(z)$ is the displacement operator. The interaction time for each operation R_θ is $T = \theta/(6g)$, which is expected to yield states with $\bar{n} = 9$. **b** Gate error for an X_π operation as a function of the average photon number \bar{n} of the drive pulse which is initialized either in the coherent state (red color) or the squeezed cat state (blue color). The highlighted areas indicate the range of error, depending on the initial state of the qubit, and the solid lines show the error averaged over qubit states distributed uniformly on the Bloch sphere, $\bar{\mathcal{E}}$. The inset shows the difference $\Delta\mathcal{E}$ between the numerically calculated errors and their analytical first-order approximations (Table 1), with dashed lines indicating the difference in maximum errors

Table 1. Analytical expressions for gate errors using different drive states

State	R'_π			$R'_{\pi/2}$		
	$\bar{\mathcal{E}}$	\mathcal{E}_{max}	r	$\bar{\mathcal{E}}$	r	
Coherent, $ \sqrt{\bar{n}}e^{i\phi}\rangle$	$\frac{4+\pi^2}{24\bar{n}}$	(110%)	$\frac{4+4\pi+\pi^2}{16\bar{n}}$	$\frac{8+\pi^2}{96\bar{n}}$	(100.5%)	0
Squeezed, $ \sqrt{\bar{n}}e^{i\phi}, r\rangle$	$\frac{\pi}{6\bar{n}}$	(*)	$\frac{\pi}{2\bar{n}}$	$\frac{\sqrt{2}\pi}{24\bar{n}}$	(*)	$e^{2i\phi} \ln \sqrt{\pi/2}$
S. cat, $ \sqrt{\bar{n}}e^{i\phi}, r\rangle \pm -\sqrt{\bar{n}}e^{i\phi}, r\rangle$	$\frac{\pi}{6\bar{n}}$	(*)	$\frac{\pi}{4\bar{n}}$	(*)	(*)	$e^{2i\phi} \ln \sqrt{\pi/2}$

Note: Average and maximum errors for gates R'_π and $R'_{\pi/2}$ to the first order in \bar{n}^{-1} , implemented with the drive pulse either in a coherent state, in a squeezed coherent state, or in a squeezed cat state. Here, R' lies in the xy-plane forming an angle ϕ with respect to the x-axis. The squeezing parameter, r , is chosen in each case to minimize the average error $\bar{\mathcal{E}}$. The percentages denote the error in units of the lower bounds marked with (*)

optimal squeezing parameters, are equal to those obtained in the semiclassical approach above.

In the specific case of π -rotations, a sum of two eigenvectors, i.e., the squeezed cat state^{28–30}

$$|\Sigma(a)\rangle = \frac{1}{\mathcal{N}} \left(|a, \ln \sqrt{\pi/2}\rangle \pm |-a, \ln \sqrt{\pi/2}\rangle \right), \quad (6)$$

where the positive constant \mathcal{N} ensures normalization, is a state that minimizes both the average and the maximum error simultaneously (see [Supplementary Information](#)). Comparison of errors produced by such a state and a coherent state is presented in Fig. 2b.

Generally for R'_θ gates, we find solutions with errors that vanish as $1/\bar{n}$ in the limit $\bar{n} \rightarrow \infty$, as shown in the [Supplementary Information](#). The lower bounds together with errors induced by non-squeezed coherent states are shown in Table 1. Other gates, such as the Pauli-Z gate and the Hadamard gate, can be constructed as sequences of R'_θ gates. Recently, it was shown that squeezing also improves the fidelity of the phase gate in the dispersive regime.³¹

Drive-refreshing protocol

All of the fundamental lower bounds derived above are inversely proportional to the average photon number. Intuitively, a drive with a large photon number should be capable of inducing

multiple gates without changing substantially, thus decreasing the required amount of energy per gate for nearly equal error level. We show below that reusing a drive effectively decreases the energy consumption well below the lower bound of average gate error for disposable pulses. Furthermore, the drive can be corrected between successive gates such that the consumption drops without essential decrease of the average gate fidelity.

In our protocol, an itinerant control drive cyclically interacts with a register of resonant qubits and ancillary qubits, see Fig. 3a. A cycle begins with the drive, initially in a suitable squeezed coherent state, applying a chosen gate operation with minimal error on a register qubit. Consequently, the drive state changes due to the quantum back-action. To undo this, the drive is set to sequentially interact with corrective ancilla qubits, initialized in a superposition of ground and excited states, for a time corresponding to a π -rotation. As a result, the purity, energy, and phase of the drive are restored in successive interactions (see [Supplementary Information](#)). At the end of the cycle, the ancilla qubits are reset and the refreshed drive is usable for another high-fidelity gate.

Insight into the refreshing mechanism of the ancillary interactions can be obtained by considering the path traversed by the Bloch vector of the ancillary qubit, as illustrated in Fig. 3b. A drive lacking energy rotates the vector with smaller angular frequency, leaving the ancilla slightly biased towards the ground state and gaining energy in the process. Similarly, excessive energy in the

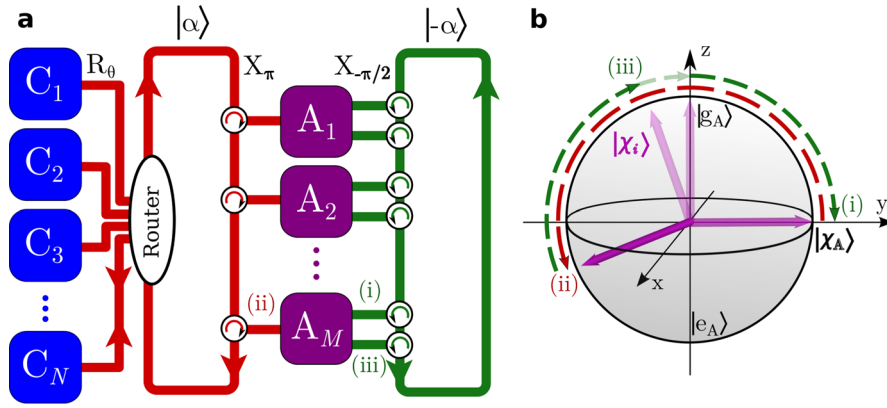


Fig. 3 **a** Schematic diagram of the drive-refreshing protocol. During a single cycle, the itinerant drive pulse (red) induces a chosen rotation R_θ on one of the qubits C_i in the register and is then refreshed by sequential X_π interactions with each ancillary qubit $\{A_j\}$. In an ideal setting, each ancilla is prepared precisely into the state $(|g_A\rangle + i|e_A\rangle)/\sqrt{2}$ and reset after each cycle. Alternatively, the ancilla qubits are initially in their ground states and their imperfect preparation and reset is implemented by an itinerant corrector pulse (green). **b** Evolution of an ancilla state during a refreshing cycle: (i) preparation from the ground state into the state $|\chi_A\rangle = (|g_A\rangle + i|e_A\rangle)/\sqrt{2}$, (ii) drive refresh as a result the primary rotation (red), and (iii) ancilla reset. We either assume that the preparative steps (i) and (iii) are ideal or induced by a corrector pulse

drive is transferred to the ancilla due to rotating it closer to the excited state. This effect is discussed further in the [Supplementary Information](#).

With increasing number of ancilla qubits, the execution time of a full cycle increases and thus a single itinerant pulse applies a gate on the register less frequently. To compensate for this, one may use as many drive pulses as there are ancillas in the array, and synchronize their travel times such that each qubit interacts with one of the pulses at a given time. Such a system is able to apply as many gates on the register per cycle as there are itinerant pulses in circulation. However, we restrict our analysis to a single itinerant pulse.

Simplified implementation with ideally prepared ancilla

During one cycle of our protocol, a single drive first interacts with a register qubit, followed by M interactions with ancilla qubits each prepared in the state $(|g_A\rangle + i|e_A\rangle)/\sqrt{2}$. To gain theoretical insight into the core idea of the protocol, we first consider a simplified version where the ancilla qubits are perfectly prepared and reset for every cycle. Additionally, we assume that the register qubits are uncorrelated, and that their states are uniformly randomized over the Bloch sphere.

We numerically simulate the evolution of the drive and evaluate the average error of the gate X_π for a register qubit after each cycle. See Methods for a step-by-step description of the simulation. During the simplified protocol, the average error $\bar{\epsilon}$ will increase from its initial lower-bound value at varying rates depending on the states of the register qubits. We find that after many cycles, the drive reaches a steady state that generates the desired gates with a predictable average error. With 1–3 ancillas per cycle, the average error saturates after a hundred cycles; with ten or more ancillas, the saturation takes less than ten cycles. If no corrective ancillas are used, the average error eventually reaches 0.5.

Figure 4a shows how the eventual error level depends on the number of photons and ancillas. The average gate error approaches its theoretical lower bound, in the limit of many drive-refreshing ancilla qubits. For smaller rotation angles, qualitatively similar results are obtained with more slowly accumulating error. Thus a single itinerant drive pulse supplied with ideal ancilla states can generate an infinite number of high-fidelity gates.

Register in an entangled state

Above, the qubits in the register were assumed to be essentially uncorrelated. Here we demonstrate the beneficial performance of our method in the case where the register qubits are maximally entangled. We initialize the register of N qubits in the Greenberger–Horne–Zeilinger (GHZ) state $|\psi_{\text{GHZ}}\rangle = (|g\rangle^{\otimes N} + |e\rangle^{\otimes N})/\sqrt{2}$. The control method itself is identical to the one used above: the drive interacts with only one qubit at a time to implement a single-qubit gate \hat{K} and is subsequently refreshed by M ideally prepared ancillas between each such gate. The target operation on the register is thus $\hat{K}^{\otimes N}$. After the drive has interacted with every register qubit once, the state of the register has transformed into $\tilde{\rho}$ and the total transformation error is computed as

$$\mathcal{E}_{\text{GHZ}} = 1 - \text{Tr}[\tilde{\rho} \hat{K}^{\otimes N} |\psi_{\text{GHZ}}\rangle \langle \psi_{\text{GHZ}}| (\hat{K}^\dagger)^{\otimes N}]. \quad (7)$$

We divide this error by the number of qubits to obtain the effective error per gate, $\mathcal{E}_{\text{eff}} = \mathcal{E}_{\text{GHZ}}/N$.

Results of a simulation for an $X_{\pi/2}$ gate with the initial drive state $|\sqrt{100}, \ln\sqrt{\pi/2}\rangle$ are shown in Fig. 4b. A behavior similar to Fig. 4a is observed: with enough ancillary corrections between the register gates, the error produced by an itinerant drive can be reduced to the level given by individual optimal pulses. The figure also suggests that even without corrections, reusing a drive of certain energy is more beneficial in practice than dividing the same amount of photons into individual, weaker disposable pulses. Thus we conclude that regardless of the state of the register, refreshment of a drive pulse likely serves to improve the trade-off between gate error and required energy.

The above case of entangled qubits, with the chosen target gate $X_{\pi/2}$, provides a way to compare our results to the previous work by Gea-Banacloche and Ozawa,¹⁶ where they studied a register in a GHZ state that was driven by \bar{n} photons on average. They showed that the maximum gate error of the $X_{\pi/2}$ rotation for each qubit in this system scales as N/\bar{n} . This scaling was used to argue that a pulse of average photon number \bar{n}_{total} cannot outperform N individual pulses of \bar{n}_{total}/N average photons, although their performance was not compared explicitly. The key differences here are that Ref. 16 does not consider the possibility of using ancillary qubits, and that it employs a definition of error which also accounts for the infidelity of the drive state. Our results suggest that the errors due to both reused and disposable pulses of equal total energy increase sublinearly with N , the prefactor for reused pulses is much smaller than for

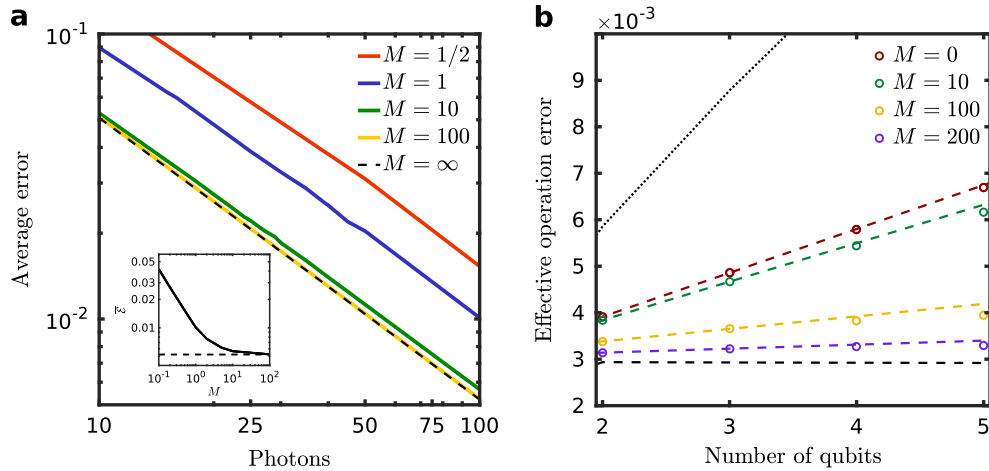


Fig. 4 **a** Average error $\bar{\mathcal{E}}$ of X_π gates generated by an itinerant drive pulse which initially had an average photon number \bar{n} and has reached the steady state due to ancilla refreshing. The drive is set to interact with M ideal ancillas ($|X_A\rangle = (|g_A\rangle + i|e_A\rangle)/\sqrt{2}$) per cycle as indicated, leading to effective refreshing of the drive state. The *dashed line* indicates the lower bound of error which is achieved either with a disposable optimal pulse or with a pulse refreshed by infinitely many ideal ancillas. The inset shows the average gate error as a function of M for $\bar{n} = 100$. **b** State preparation error per qubit $\mathcal{E}_{\text{eff}} = \mathcal{E}_{\text{GHZ}}/N$ for a register of N qubits initially in a GHZ state. The target gate is an $X_{\pi/2}$ rotation for all qubits individually, implemented by a squeezed state of $\bar{n} = 100$ photons ($r = \ln \sqrt{\pi/2}$) that is refreshed by M ideal ancillas per cycle. The *circles* represent the data, whereas the *colored lines* extend the line segments between the first two data points, to distinguish deviations from linear behavior. The *black dashed line* represents the error obtained using N disposable pulses of constant photon number $\bar{n} = 100$. The *dotted line* is the error due to disposable pulses of constant total energy $\bar{n} = 100/N$

disposable pulses, and the prefactor can be greatly improved by the refreshing protocol.

Full protocol

The total energy consumption of the protocol can be meaningfully estimated only if the method and energy cost of the ancilla preparation and reset are specified. To this end, we propose to prepare the ancillas by an itinerant corrector pulse shown in Fig. 3a. In the full protocol, the ancilla qubits are first prepared in their ground state and then controlled by the corrector pulse from cycle to cycle. With opposite phase and half the interaction time compared with the drive, the corrector pulse applies an $X_{-\pi/2}$ gate on the ancilla before and after an X_π gate introduced by the drive pulse, see Methods for details. The purpose of the last $X_{-\pi/2}$ gate is to return the ancilla qubit close to the ground state, thus performing an imperfect reset. For simplicity, we assume that the state of the register is separable.

Since all ancilla qubits are prepared to the ground state, the energy consumption fully arises from the drive and corrector pulses, both of which have the initial average energy $\bar{n}\hbar\omega$. Thus, the average energy consumption per register gate is $E = 2\hbar\omega\bar{n}/N$, where N is the number of transformed register qubits, or equally the number of elapsed cycles. In the case where the drive-refreshing protocol is not used, $M = 0$, we have $E = \bar{n}\hbar\omega/N$.

The evolution of the drive state depends on the randomized sequence of the initial states of the register qubits. Results from multiple simulations are averaged and shown in Fig. 5. In contrast to the ideal case, the system accumulates error over repeated cycles and the average gate error does not saturate. The accumulation of error is attributed to imperfect preparations and resets of the ancillas as well as accumulating entanglement between the drive and ancilla states. Nevertheless, we find that with a sufficient number of ancillary qubit interactions between the register gates, the average error remains nearly constant for a large number of successive gates. The protocol can be stopped before the error reaches a desired threshold. This shows that the total energy cost per register gate is effectively reduced to orders of magnitude below the lower bound for disposable pulses. In fact, Fig. 5 suggests that the gate error may be, in theory, reduced

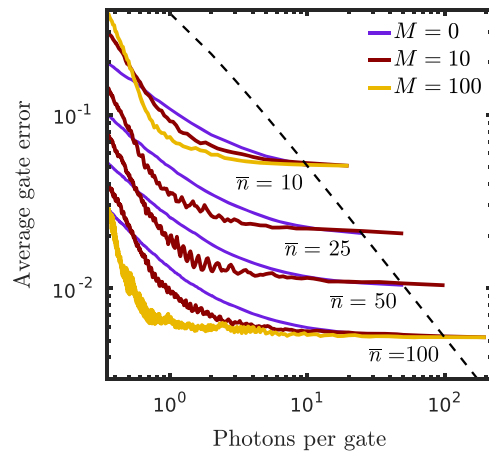


Fig. 5 Average gate error as a function of the photon cost per gate, $2\bar{n}/N$ for $M > 0$ and \bar{n}/N for $M = 0$. Here, \bar{n} is the mean number of photons in the initial pulses and N is the number of X_π register gates generated by the protocol. The ancilla states are non-ideally prepared by a corrector pulse initially in state $|\sqrt{\pi/2}, \ln \sqrt{\pi/2}\rangle$. During the protocol, the curve advances from *right to left* as $1/N$ decreases. The results are averaged over multiple simulations. The *dashed line* indicates the lower bound of error which is achieved with a single disposable optimal pulse

indefinitely without increasing the power consumption by using more energetic pulses.

DISCUSSION

In this work, we derived the greatest lower bound for the error of a single-qubit gate implemented with a single resonant control mode of a given mean energy. In contrast to previous work, our method for obtaining the bound is not restricted to any particular gate or state of the qubit-drive system. The method can also be used to find the quantum state of the drive mode that minimizes

the average gate error, or alternatively the transformation error for a chosen initial qubit state. Specifically, we found that the lower bounds for rotations about axes in the xy -plane are achieved by squeezing the quantum state of a coherent drive pulse by an amount that depends on the target gate. Together with the recent result that squeezing also significantly improves the phase gate in the dispersive regime,³¹ our results suggest that squeezing may generally yield useful improvements in different control schemes. This calls for experimental studies on outperforming the widely-used coherent state.

Importantly, our results also impose a lower bound on the energy consumption of qubits controlled by individual disposable pulses. However, we theoretically introduced a protocol where a control pulse is used to generate multiple gates and is refreshed between them to avoid loss of gate fidelity. This protocol exhibits orders of magnitude lower power consumption than the bound for disposable pulses. The refreshing process may also prove useful in correcting the phase and amplitude errors of a noisy control pulse.

Our protocol can possibly be realized in some form with future low-loss microwave components such as photon routers,^{32, 33} circulators, and nanoelectromechanical systems.³⁴ Technical limitations in the quality of these devices will set in practice the trade-off between the achievable gate fidelity and the dissipated power. In the future, our work can be extended to error bounds for 2-qubit gates, state preservation, pulse amplification, and propagating control pulses composed of a continuum of bosonic modes.

METHODS

Gate error in the Jaynes–Cummings model

The dynamics of the qubit–drive system is generally described by the Jaynes–Cummings Model,^{20, 21} which includes the rotating-wave approximation. Assuming resonant interaction, the system is governed by the interaction Hamiltonian

$$\hat{H}_{\text{int}} = \hbar g(t)(|e\rangle\langle g| \otimes \hat{a} + |g\rangle\langle e| \otimes \hat{a}^\dagger), \quad (8)$$

where \hat{a} is the bosonic annihilation operator of the drive mode. Without loss of generality, we assume an on-off envelope such that $g(t) = \text{const.}$ for $0 < t < T$ and $g(t) = 0$ otherwise. Most features of the semiclassical model are reobtained if $|a| \rightarrow \infty$ and the drive is in the coherent state $|a\rangle = e^{-\frac{1}{2}|a|^2} \sum_{n=0}^{\infty} \frac{a^n}{\sqrt{n!}} |n\rangle$, where $|n\rangle$ is the n th Fock state. For example, taking the expectation value of \hat{H}_{int} in the state $|a\rangle$ yields the semiclassical Hamiltonian in Eq. (1). Thus the coherent state approximately induces a gate R_θ if the timing condition $2gT|a| = \theta$ is satisfied.

In contrast to the semiclassical model, the evolution of the qubit is not unitary. After the interaction, the qubit state is extracted by taking a partial trace over the drive degrees of freedom as

$$\hat{\chi}(T) = \text{Tr}_D[\hat{U}(T)\hat{\rho}_0\hat{U}^\dagger(T)], \quad (9)$$

where $\hat{\rho}_0$ and $\hat{U}(T)$ denote the arbitrary initial density operator and the evolution operator of the qubit–drive system, respectively. The error, or infidelity, between the target and the resulting qubit state is here defined as

$$\mathcal{E}[\hat{\chi}_0, \hat{\chi}(T)] = 1 - \text{Tr}[\hat{\chi}(T)\hat{\chi}_0\hat{\chi}^\dagger], \quad (10)$$

which can be regarded as a generalization of Eq. (2).

Minimization of gate error

If the initial state of the joint system is separable and pure, $\hat{\rho}_0 = |\chi_0\rangle\langle\chi_0| \otimes |\sigma_0\rangle\langle\sigma_0|$, where $|\chi_0\rangle$ and $|\sigma_0\rangle$ denote the initial qubit and drive states, respectively, the gate error of Eq. (4) induced by the Jaynes–Cummings interaction can be written in the general form (see [Supplementary Information](#) for derivation)

$$\mathcal{E}_i(\sigma_0) = 1 - \langle\sigma_0|\hat{F}_i|\sigma_0\rangle. \quad (11)$$

Here, \mathcal{E}_i denotes either the transformation error $\mathcal{E}(\vartheta, \varphi)$ of a particular qubit state, the average gate error $\bar{\mathcal{E}}$ [Eq. (3)], or the maximum gate error \mathcal{E}_{max} . The information about the desired gate and chosen interaction time

is contained in the corresponding operator \hat{F}_i which is denoted either by $\hat{F}(\vartheta, \varphi)$, \hat{F}_{avg} , or \hat{F}_{max} , respectively. An analytical expression for $\hat{F}(\vartheta, \varphi)$ and \hat{F}_{avg} can be found for any gate, whereas an expression for \hat{F}_{max} exists for at least rotations R'_{π} , where the rotation axis R' is restricted to the xy -plane of the Bloch sphere. See [Supplementary Information](#) for derivations and detailed expressions. From Eq. (11) we see that the error-minimizing drive states are the eigenstates of operators \hat{F}_i that correspond to the largest eigenvalue f_i ,

$$\hat{F}_i|\sigma_0^{\text{opt},i}\rangle = f_i|\sigma_0^{\text{opt},i}\rangle \quad (12)$$

The numerical approach for solving the eigenstates of \hat{F}_i has the disadvantage of truncating the infinite-dimensional state vector to a finite vector of length N_{cut} , which might distort or exclude some of the possible solutions. However, the obtained Gaussian-like solutions are not affected by changes in the cut-off for $N_{\text{cut}} - \bar{n} \gg \sqrt{\bar{n}}$. Raising the cut-off reveals more energetic solutions, but these correspond to pulses that implement the chosen gate after an integer number of unnecessary 2π rotations.

Simplified refreshing protocol with ideal preparations

The Hilbert space of the drive-refreshing system is formally a composite space of the Fock space D of the drive and the two-level spaces $\{|Q_k\rangle_k = \{|C_i\rangle A_j\}_{i,j}$ of the register and ancilla qubits,

$$\mathcal{S} = \left(\bigotimes_{k=1}^{N+M} Q_k \right) \otimes D = \left(\bigotimes_{i=1}^N C_i \right) \otimes \left(\bigotimes_{j=1}^M A_j \right) \otimes D. \quad (13)$$

The drive only interacts with one qubit at a time and therefore each interaction can be calculated in the subspace of the relevant qubit and the drive, assuming the qubits are not correlated. After the interaction, the drive state is extracted by tracing over the associated qubit space. Namely, the i th iteration of the drive state is given by

$$\hat{\sigma}_{i+1} = \text{Tr}_Q[\hat{U}_i(|\chi_i\rangle\langle\chi_i| \otimes \hat{\sigma}_i)\hat{U}_i^\dagger], \quad (14)$$

where \hat{U}_i acts in the subspace of the drive and the i th qubit in the control sequences described below.

For the target gate X_m , the simplified protocol without the additional corrector pulse is executed with the following steps:

- (i) The drive state is initialized to the state $\sigma_0 = |\sqrt{n}, \ln \sqrt{\pi/2}\rangle$.
- (ii) A new register qubit is initialized in a random pure state, chosen uniformly from the Bloch sphere.
- (iii) The drive interacts with the register qubit for interaction time $T = \pi/(2g\bar{n})$ [Eq. (14)].
- (iv) The M ancilla qubits are initialized to $|\chi_A\rangle = (|g_A\rangle + i|e_A\rangle)/\sqrt{2}$.
- (v) The drive interacts with an ancilla qubit for interaction time $T = \pi/(2g\bar{n})$. Repeat for all ancillas.
- (vi) Evaluate the average error $\bar{\mathcal{E}}$ of a hypothetical X_m gate with Eqs (3) and (4) using the current drive state. Continue from step (ii).

For gates other than X_m , the phases of the drive and ancillas, as well as the interaction time in step (iii), but not step (v), would be shifted accordingly.

Register in an entangled state

In the case where the register is initialized in the GHZ state, the temporal evolution operators must be calculated in the Hilbert space $(\bigotimes_{i=1}^N C_i) \otimes D$ or $(\bigotimes_{i=1}^N C_i) \otimes A_j \otimes D$ for interactions between the drive and a register qubit, or drive and the j th ancilla, respectively. No partial trace over any register qubit is taken. Although the physical control scheme is the same as for the non-entangled register, the simulation differs in steps (ii) and (vi). To obtain a convenient comparison with Ref. 16, the target gate is chosen as $X_{m/2}$. The simulation proceeds by the following steps:

- (i) The drive state is initialized to the $\bar{\mathcal{E}}$ -minimizing state $|\sigma_0\rangle = |\sqrt{n}, \ln \sqrt{\pi/2}\rangle$.
- (ii) The register is initialized in the GHZ state $(|g\rangle^{\otimes N} + |e\rangle^{\otimes N})/\sqrt{2}$.
- (iii) The drive interacts with a register qubit for interaction time $T/2 = \pi/(4g\bar{n})$ [Eq. (14)].
- (iv) The M ancilla qubits are initialized to $|\chi_A\rangle = (|g_A\rangle + i|e_A\rangle)/\sqrt{2}$.
- (v) The drive interacts with an ancilla qubit for interaction time $T = \pi/(2g\bar{n})$. Repeat for all ancillas.
- (vi) Continue from step (iii), unless the drive has interacted with every register qubit.
- (vii) Evaluate the transformation error using Eq. (7).

Full protocol

In the full protocol, a corrector pulse is added to the system to prepare the ancilla qubits and we assume that the register is initially in a separable state. In addition to computing the drive state after each ancilla interaction, the state of the interacting ancilla qubit is also extracted for subsequent use by a partial trace over the drive degrees of freedom. This is justified if the ancilla qubits do not become strongly correlated during the evolution. This approximation is more accurate the closer the control pulses are to classical pulses which do not induce entanglement.

The full protocol is given by:

- (i) The drive state is initialized to $|\sqrt{n}, \ln \sqrt{\pi/2}\rangle$, the corrector pulse to $|\sqrt{n}, \ln \sqrt{\pi/2}\rangle$ and all M ancillas to the ground state.
- (ii) A new register qubit is initialized in a random pure state.
- (iii) The drive interacts with the register qubit with interaction time $T = \pi/(2g\bar{n})$ [Eq. (14)].
- (iv) An ancilla qubit interacts sequentially with the corrector, the drive, and the corrector again, with interaction times $T/2$, T , and $T/2$, respectively. Repeat for all other ancillas.
- (v) Evaluate the average error $\bar{\mathcal{E}}$ of a hypothetical X_π gate with Eqs (3) and (4) using the current drive state. Continue from step (ii).

ACKNOWLEDGEMENTS

We thank Paolo Solinas and Benjamin Huard for useful discussions. This work was supported by the European Research Council under Starting Independent Researcher Grant No. 278117 (SINGLEOUT) and under Consolidator Grant No. 681311 (QUESS). We also acknowledge funding from the Academy of Finland through its Centers of Excellence Program (grant nos 251748 and 284621) and grant (no. 286215) and from the Finnish Cultural Foundation.

COMPETING INTERESTS

The authors declare no competing interests.

REFERENCES

1. Preskill, J. Reliable quantum computers. *Proc. R. Soc. Lond. A* **454**, 385–410 (1998). <http://rspa.royalsocietypublishing.org/content/454/1969/385>
2. Nakamura, Y., Pashkin, Y. A. & Tsai, J. S. Coherent control of macroscopic quantum states in a single-cooper-pair box. *Nature* **398**, 786–788, doi:10.1038/19718 (1999).
3. Barends, R. et al. Superconducting quantum circuits at the surface code threshold for fault tolerance. *Nature* **508**, 500–503, doi:10.1038/nature13171 (2014).
4. Kelly, J. et al. State preservation by repetitive error detection in a superconducting quantum circuit. *Nature* **519**, 66–69, doi:10.1038/nature14270 (2015).
5. Bonadeo, N. H. et al. Coherent optical control of the quantum state of a single quantum dot. *Science* **282**, 1473–1476 (1998). <http://science.sciencemag.org/content/282/5393/1473>
6. Veldhorst, M. et al. A two-qubit logic gate in silicon. *Nature* **526**, 410–414, doi:10.1038/nature15263 (2015).
7. Sackett, C. A. et al. Experimental entanglement of four particles. *Nature* **404**, 256–259, doi:10.1038/35005011 (2000).
8. Debnath, S. et al. Demonstration of a small programmable quantum computer with atomic qubits. *Nature* **536**, 63–66, doi:10.1038/nature18648 (2016).
9. Pla, J. J. et al. A single-atom electron spin qubit in silicon. *Nature* **489**, 541–545, doi:10.1038/nature11449 (2012).
10. Togan, E. et al. Quantum entanglement between an optical photon and a solid-state spin qubit. *Nature* **466**, 730–734, doi:10.1038/nature09256 (2010).
11. Terhal, B. M. Quantum error correction for quantum memories. *Rev. Mod. Phys.* **87**, 307–346, doi:10.1103/RevModPhys.87.307 (2015).
12. Fowler, A. G., Mariantoni, M., Martinis, J. M. & Cleland, A. N. Surface codes: towards practical large-scale quantum computation. *Phys. Rev. A* **86**, 032324, doi:10.1103/PhysRevA.86.032324 (2012).
13. Ozawa, M. Conservative quantum computing. *Phys. Rev. Lett.* **89**, 057902, doi:10.1103/PhysRevLett.89.057902 (2002).
14. Gea-Banacloche, J. Minimum energy requirements for quantum computation. *Phys. Rev. Lett.* **89**, 217901, doi:10.1103/PhysRevLett.89.217901 (2002).

15. Gea-Banacloche, J. & Ozawa, M. Constraints for quantum logic arising from conservation laws and field fluctuations. *J. Opt. B* **7**, S326 (2005). <http://stacks.iop.org/1464-4266/7/i=10/a=017>
16. Gea-Banacloche, J. & Ozawa, M. Minimum-energy pulses for quantum logic cannot be shared. *Phys. Rev. A* **74**, 060301, doi:10.1103/PhysRevA.74.060301 (2006).
17. Gea-Banacloche, J. & Miller, M. Quantum logic with quantized control fields beyond the $1/n$ limit: mathematically possible, physically unlikely. *Phys. Rev. A* **78**, 032331, doi:10.1103/PhysRevA.78.032331 (2008).
18. Karasawa, T., Gea-Banacloche, J. & Ozawa, M. Gate fidelity of arbitrary single-qubit gates constrained by conservation laws. *J. Phys. A* **42**, 225303 (2009). <http://stacks.iop.org/1751-8121/42/i=22/a=225303>
19. Iqeta, K., Imoto, N. & Koashi, M. Fundamental limit to qubit control with coherent field. *Phys. Rev. A* **87**, 022321, doi:10.1103/PhysRevA.87.022321 (2013).
20. Jaynes, E. T. & Cummings, F. W. Comparison of quantum and semiclassical radiation theories with application to the beam maser. *Proc. IEEE* **51**, 89–109 (1963).
21. Shore, B. W. & Knight, P. L. The jaynes-cummings model. *J. Mod. Opt.* **40**, 1195–1238 (1993).
22. Layden, D., Martn-Martnez, E. & Kempf, A. Universal scheme for indirect quantum control. *Phys. Rev. A* **93**, 040301, doi:10.1103/PhysRevA.93.040301 (2016).
23. Slosser, J. J., Meystre, P. & Braunstein, S. L. Harmonic oscillator driven by a quantum current. *Phys. Rev. Lett.* **63**, 934–937, doi:10.1103/PhysRevLett.63.934 (1989).
24. Åberg, J. Catalytic coherence. *Phys. Rev. Lett.* **113**, 150402, doi:10.1103/PhysRevLett.113.150402 (2014).
25. Nakahara, M. & Ohmi, T. *Quantum computing: From linear algebra To physical realizations* (CRC Press, 2008).
26. Pegg, D. T. & Barnett, S. M. Phase properties of the quantized single-mode electromagnetic field. *Phys. Rev. A* **39**, 1665–1675, doi:10.1103/PhysRevA.39.1665 (1989).
27. Salmilehto, J., Solinas, P. & Möttönen, M. Quantum driving and work. *Phys. Rev. E* **89**, 052128, doi:10.1103/PhysRevE.89.052128 (2014).
28. Dodonov, V. V. 'Nonclassical' states in quantum optics: a 'squeezed' review of the first 75 years. *J. Opt. B* **4**, R1 (2002). <http://stacks.iop.org/1464-4266/4/i=1/a=201>
29. Govia, L. C. G., Pritchett, E. J. & Wilhelm, F. K. Generating nonclassical states from classical radiation by subtraction measurements. *New J. Phys.* **16**, 045011 (2014). <http://stacks.iop.org/1367-2630/16/i=4/a=045011>
30. Vlastakis, B. et al. Deterministically encoding quantum information using 100-photon schrödinger cat states. *Science* **342**, 607–610 (2013). <http://science.sciencemag.org/content/342/6158/607>
31. Puri, S. & Blais, A. High-fidelity resonator-induced phase gate with single-mode squeezing. *Phys. Rev. Lett.* **116**, 180501, doi:10.1103/PhysRevLett.116.180501 (2016).
32. Pechal, M. et al. Superconducting switch for fast on-chip routing of quantum microwave fields. *Phys. Rev. Appl.* **6**, 024009, doi:10.1103/PhysRevApplied.6.024009 (2016).
33. Hoi, I.-C. et al. Demonstration of a single-photon router in the microwave regime. *Phys. Rev. Lett.* **107**, 073601, doi:10.1103/PhysRevLett.107.073601 (2011).
34. Zhou, X. et al. Slowing, advancing and switching of microwave signals using circuit nanoelectromechanics. *Nat. Phys.* **9**, 179–184, doi:10.1038/nphys2527 (2013).



Open Access This article is licensed under a Creative Commons Attribution 4.0 International License, which permits use, sharing, adaptation, distribution and reproduction in any medium or format, as long as you give appropriate credit to the original author(s) and the source, provide a link to the Creative Commons license, and indicate if changes were made. The images or other third party material in this article are included in the article's Creative Commons license, unless indicated otherwise in a credit line to the material. If material is not included in the article's Creative Commons license and your intended use is not permitted by statutory regulation or exceeds the permitted use, you will need to obtain permission directly from the copyright holder. To view a copy of this license, visit <http://creativecommons.org/licenses/by/4.0/>.

© The Author(s) 2017

Supplementary Information accompanies the paper on the *npj Quantum Information* website (doi:10.1038/s41534-017-0015-5).